Current-voltage relation of a centrifugally confined plasma

L. C. Ray,[1] Y.-J. Su,[2] R. E. Ergun,[1] P. A. Delamere,[1] and F. Bagenal[1]

Received 5 December 2008; revised 5 February 2009; accepted 9 February 2009; published 28 April 2009.

[1] Observations of Jupiter's auroral regions indicate that electrons are accelerated into Jupiter's atmosphere creating emissions. The acceleration of the electrons intimate that parallel electric fields and field-aligned currents develop along the flux tubes which connect the equatorial plane to the areas with auroral emission. The relationship between the development of parallel electric fields and the parallel currents is often assumed to be the same as that on Earth. However, the relationship is significantly different at Jupiter due to a lack of plasma at high latitudes as large centrifugal forces caused by Jupiter's fast rotation period (about 9.8 h) constrain the magnetospheric plasma to the equatorial plane. We use a 1-D spatial, 2-D velocity space Vlasov code which has been modified to include centrifugal forces to examine the current-voltage relationship that exists at Jupiter. In particular, we investigate this relationship at a distance of 5.9 Jovian radii, the orbital radius of Io, which is coupled with the auroral spot and Io wake auroral emissions.

Citation: Ray, L. C., Y.-J. Su, R. E. Ergun, P. A. Delamere, and F. Bagenal (2009), Current-voltage relation of a centrifugally confined plasma, *J. Geophys. Res.*, *114*, A04214, doi:10.1029/2008JA013969.

1. Introduction

[2] The primary acceleration mechanism in the upward current region of the aurora is parallel electric fields. At Earth, this has been inferred by sounding rocket observations in auroral regions [*Evans*, 1974; *Mozer and Kletzing*, 1998] and directly observed by satellites [*Mozer and Kletzing*, 1998; *Ergun et al.*, 1998]. The relationship between parallel electric fields and field-aligned current was theoretically explored by *Knight* [1973] for the Earth case. *Knight* [1973] found that parallel electric fields, and hence field-aligned potentials are related to currents carried by electrons that move against the mirror force in the Earth's magnetosphere. The enhanced current results in strong parallel electric fields which drive electron beams that excite atmospheric emissions, including observable auroral emissions. *Ergun et al.* [2000] modeled the potential structure in the upward current region using a steady state 1-D spatial 2-D velocity space code. Their analysis validated the *Knight* [1973] current-voltage relation at Earth.

[3] However, the *Knight* [1973] analysis is for a system in which the motion of particles along the magnetic field line is dictated by the magnetic mirror force. At Earth, the plasma density distribution along the field line is determined by gravitational forces, and thus monotonically decreases toward the equatorial plane. However for a rapidly rotating system, such as Jupiter or Saturn with rotational periods of $\sim$9.8 h and $\sim$10.6 h, respectively, centrifugal forces are significant and affect the plasma density distribution along the field. Heavy ions are confined to the equator causing a minimum in the plasma density at high latitudes, roughly $\sim$2–3 planetary radii from the planet's center. The ions are more strongly confined than are the electrons, resulting in an ambipolar electric field. The subsequent potential structure along the field line is not monotonic between the ionosphere and the magnetosphere, violating one of the assumptions of the *Knight* [1973] analysis.

[4] *Boström* [2003] investigated the current-voltage relation for a magnetic flux tube under general conditions, deriving the relationship using kinetic "orbital motion" theory. The analysis found that the total voltage drop along a flux tube is uniquely determined by the current density as long as particles do not mirror due to local maximums in the effective field-aligned potential (i.e., the Davisson condition is satisfied). In the case where particles are mirrored by a local maximum in the effective potential, the solution method must take into account space charge effects and the Poisson equation to determine the potential structure along the flux tube, and the relationship between the total voltage drop and current is nonunique. The *Boström* [2003] analysis looked at a broad range of voltage structures for the latter case mentioned above, including piecewise solutions where the maximum in effective potential does not occur at the plasma sheet, which is similar to the potential structure along the Io flux tube. However, ambipolar field effects were not accounted for and a solely analytic approach was applied to these solutions. We use both an analytic and Vlasov approach to investigate the nature of the current-voltage relation in this regime, focusing on the Jovian system.

[5] Jupiter's aurorae have been observed in the ultraviolet, X ray, and infrared wavelengths. In addition to the main and secondary auroral ovals, these images reveal low-latitude auroral "spots" at the footprints of the Jovian satellites, the brightest of which is associated with Io [*Clarke et al.*,

[1]Laboratory for Atmospheric and Space Physics, University of Colorado, Boulder, Colorado, USA.
[2]Department of Physics, University of Texas at Arlington, Arlington, Texas, USA.

0148-0227/09/2008JA013969

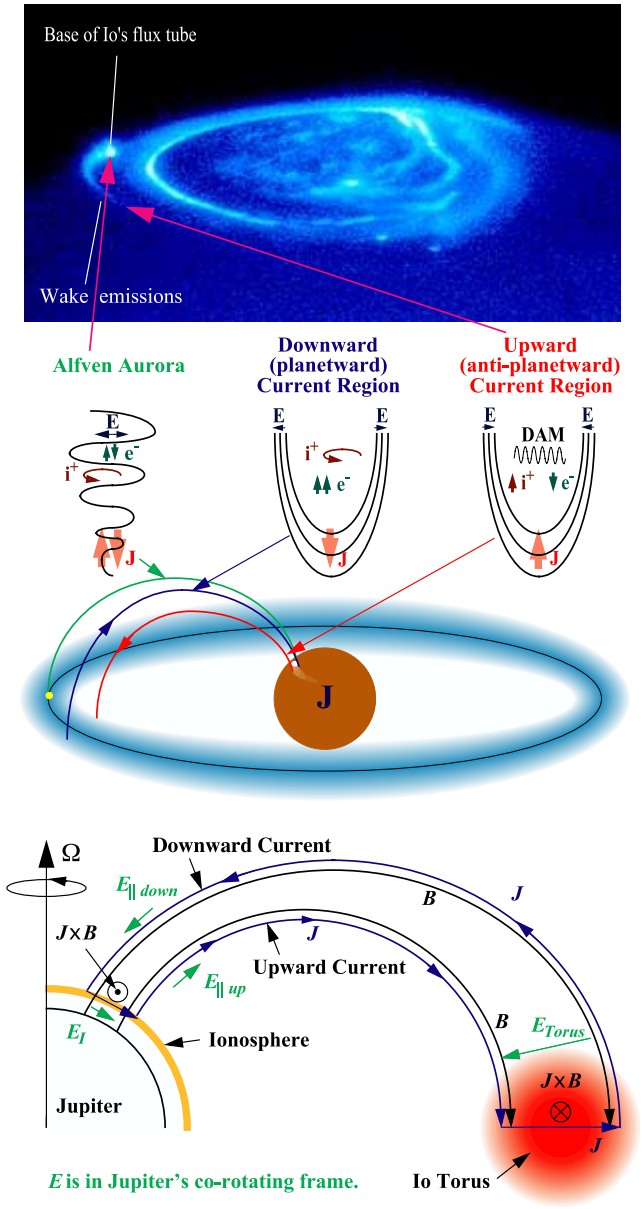

Figure 1. (top) A Jovian auroral image, where the Io-induced aurora is seen on the left with the brightest emissions at the base of the Io flux tube and an emission trail extending downstream. (middle) A depiction of the three types of auroral regions, where the green, blue, and red lines represent the Alfvénic acceleration region, the planetward current region, and the antiplanetward current region, respectively. (bottom) The quasi-static current structure downstream of Io's wake in Jupiter's corotating frame [*Su et al.*, 2003].

2004]. The main emission at Io's footprint is accompanied by an extended "wake" emission downstream of Io.

[6] Figure 1 displays a Jovian auroral image taken by the NASA Hubble Space Telescope (HST) [after *Clarke et al.*, 2002, Figure 1b]. The Io induced aurora is seen at the left with the brightest emissions at the base of the Io flux tube and a faint emission tail extending eastward. By analyzing HST Goddard High Resolution Spectrograph (GHRS) auroral spectra of the 1200–1700 Å region, *Dols et al.* [2000] suggested that the electron population responsible for the excitation of the Io footprint has a mean energy of about 60 keV. This mean energy is comparable to that of electrons beams (~75 keV) created by repeated Fermi acceleration in parallel electric fields generated by Alfvén waves [*Crary*, 1997]. *Clarke et al.* [2002] reported that 20° downstream of Io's footprint the brightness of the wake emissions is on the order of tens of kilorayleigh (kR) based on UV observations by HST. Previous studies [*Gérard et al.*, 2002; *Grodent and Gérard*, 2001; *Waite et al.*, 1983; *Gerard and Singh*, 1982] indicated that the efficiency of the electron energy conversion is close to 10 kR erg^{-1} cm^{-2} s^{-1} for primary energies between 10 and 100keV. In particular, *Gérard et al.* [2002] suggested that the mean energy for the electrons 20^o downstream of Io's footprint is ~30 keV.

[7] *Mauk et al.* [2002] indicated several similarities between the Earth's aurora and Io's auroral emission and tail. *Ergun et al.* [2002] supported this idea by suggesting that the three types of auroral acceleration regions observed by the Fast Auroral SnapshoT (FAST) at Earth, (Alfvénic acceleration region, a downward (with respect to the planet) current region, and an upward current region) are also active at Jupiter in magnetosphere-ionosphere coupling. *Delamere et al.* [2003] divided the Jupiter-Io interaction into three phases: (1) initial mass-loading interaction, (2) acceleration of the plasma in the Io wake, and (3) steady state decoupling. *Delamere et al.* [2003] suggested that the first two phases may induce an Alfvénic disturbance that is related to the bright emissions at Io's magnetic footprint, whereas the third phase sets up field-aligned currents in the downstream region of Io's wake.

[8] *Su et al.* [2003] studied the possibility that the extended tail emissions in Io's wake are due to electron acceleration in an upward current region between Jupiter and Io. Their analysis used a static kinetic Vlasov code to model electron energy fluxes and potential structures for a variety of Io torus compositions, finding that the current densities at high latitudes were strongly dependent on the hot electron population at the Io torus and the population of light ions (i.e., H^+). *Ergun et al.* [2009] models the steady state current system that develops in the Io wake region, including electric fields, field-aligned currents and subsequent auroral emission. In addition, the analysis investigates the role of parallel electric fields in the transfer of angular momentum from the ionosphere to the magnetosphere. The analysis is sensitive to the relationship between the current density and field-aligned potentials throughout the system.

[9] In this paper we explore the nature of the current-voltage relation in the Io wake region for a flux tube which intersects the equatorial plane at 5.9 R_J. We investigate a range of potential drops between the ionosphere and the magnetosphere to determine how the centrifugal confinement of the magnetospheric population affects the relationship between the current density and field-aligned potential.

2. Model Description

[10] We use the same steady state kinetic Vlasov code used by *Ergun et al.* [2000] and *Su et al.* [2003] which is one-dimensional in space and two-dimensional in velocity space, to determine a large-scale, self-consistent solution of

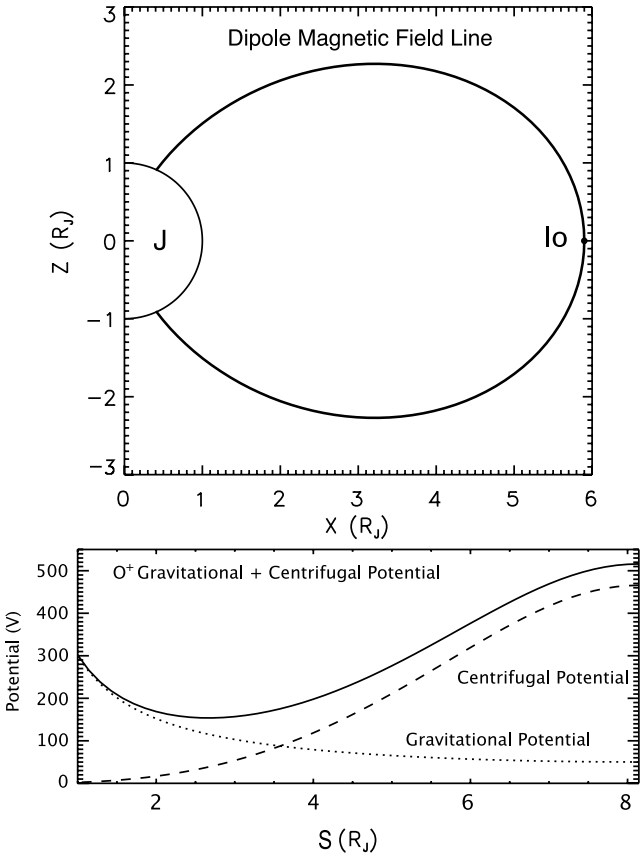

Figure 2. (top) Dipole magnetic flux tube at L = 5.9. (bottom) Gravitational and centrifugal potentials along the magnetic field line on the basis of the O^+ species.

parallel electric fields in the Io wake region. We prescribe a magnetic flux tube which runs from Jupiter's ionosphere to the equatorial plane, and intersects the equatorial plane at Io's orbital distance of L = 5.9. A set of potential drops are specified between Jupiter and the equatorial plane and subsequently adjusted to give the potential structure along the field line and current density at the ionosphere.

[11] The spatial domain, which is 1-D along the flux tube, is divided into N_s(=51) grids which are evenly spaced along the magnetic dipole field line. The Vlasov code includes the magnetic mirror effect and both gravitational and centrifugal potentials. The gravitational and centrifugal potentials based on the O^+ species are displayed in Figure 2 (bottom), with dotted and dashed lines, respectively. The solid line represents a combination of gravitational and centrifugal potentials. The horizontal axis represents Jovicentric distance in Jupiter radii (R_J). The left- and right-hand sides are the ionospheric and magnetospheric boundaries, respectively. The minimum potential is located at ~2.5 R_J along the flux tube.

[12] Cold ionospheric electrons and ions are prescribed as fluids at Jupiter's ionospheric boundary, while the Io-generated plasma species are assigned as Maxwellian distributions at the Io boundary. The only exception is the Io-generated electrons which are described as a kappa distribution to include the effects of the hot electron population. The temperature and composition of the plasma species are listed in Table 1 and described in more detail below. The distribution functions are broken into $N_v \times N_v$ velocity-space elements (N_v = 50), each of which is treated like a fluid. The potentials at the ionospheric and magnetospheric boundaries must be held fixed to represent the prescribed net potential drop. An estimated electric potential profile, Φ_s, initializes the model and then, using the set boundary conditions, the velocity space distributions are calculated along the flux tube.

[13] The model solves Poisson's equation along the field line, calculating the error at each spatial step which is defined as

$$\xi(s) = \nabla^2\Phi(s) + \frac{e}{\epsilon_0}[n_i(s) - n_e(s)] \quad (1)$$

where $n_i(s)$ and $n_e(s)$ are the ion and electron densities at each step as calculated from the distribution functions. We iteratively adjust the electric potential, Φ_s, to minimize the error $\xi(s)$, yielding a steady state solution along the field line. The spatial size of the grid ($ds \sim 10000$ km) is much larger than the Debye length ($\lambda_D < 1$ km); hence the first term on the right-hand side of the equation is negligible, essentially resulting in a quasi-neutral solution. The quasi-static model enforces adiabatic evolution without velocity-space diffusion.

[14] The Vlasov code, as applied to Earth (i.e., including gravitational forces, but excluding centrifugal forces) [*Ergun et al.*, 2000], was validated by the linear approximation to the Knight current-voltage relation [*Knight*, 1973; *Lyons*, 1980]:

$$j = K\Phi, K = \frac{e^2 n}{\sqrt{2\pi m_e T_e}} \quad (2)$$

where j and Φ are the field-aligned current density and field-aligned potential. T_e, m_e, n, and e are the electron temperature, mass, density, and charge. The current-voltage relation of *Knight* [1973] is linear in the range $1 \ll e\Phi_{\|}/k_B T_e \ll R_M$ where R_M is the mirror ratio (~400 for the Io flux tube). However, when the centrifugal confinement of particles to the equatorial plane and hence enhanced density at the equator is included, the current-voltage relation of *Knight* [1973] no longer applies (see section 3) and a new current-voltage relation is found.

3. Vlasov Solutions

3.1. Boundary Conditions

[15] The solution of the static Vlasov code is driven by boundary conditions. We choose a canonical plasma environment consistent with observations to represent the plasma conditions in the Io wake. The canonical values at the Io boundary are used to initialize the Vlasov code which then calculates the current-voltage relationship. The numerical relation is then compared to the analytic model.

[16] Cold electrons and protons are introduced at Jupiter's ionospheric boundary [*Strobel and Atreya*, 1983], while O^+, S^+, and electrons are assigned at the Io boundary. The ion composition and temperature are based on results published by *Bagenal* [1994] and *Crary et al.* [1998], with the simplification of omitting S^{++} and the minor species of O^{++} and S^{+++}. Oxygen ions are chosen to represent both

Table 1. Compositions and Temperatures of the Ion and Electron Species for All Cases

Species	Density	Temperature	Boundary
Ionospheric H^+	2×10^5 cm^{-3}	0.31 eV	left (Jupiter)
Ionospheric e^-	2×10^5 cm^{-3}	0.31 eV	left (Jupiter)
Io O^+	1750 cm^{-3}	$\parallel$ = 35 eV; $\perp$ = 70 eV	right (Io torus)
Io S^+	250 cm^{-3}	50 eV	right (Io torus)
Io e^-	2000 cm^{-3}	5 eV; $\kappa = 3$	right (Io torus)

mass/charge = 16 ion species (O^+ and S^{++}). The average temperatures of O^+ and S^+ are assumed to be 50 eV. In this paper, O^+ ions are assigned a temperature anisotropy of 2 (i.e., $T_\parallel = 35$ and $T_\perp = 70$). The number of heavy ion species has been limited in the model to minimize computer processing time. The electron temperature and distribution are based on Cassini UVIS observations of EUV emissions from the Io torus [*Steffl et al.*, 2004]. The magnetospheric electron distribution is a κ distribution with a core temperature of 5 eV and $\kappa = 3$.

[17] In addition to the plasma boundary conditions, the boundary condition of the electric potential is an important parameter in determining the current density throughout the system. Auroral emissions are a result of the high-energy precipitating electrons. We look at potential drops between the ionosphere and the magnetosphere which range from 100 V to 30 kV, consistent with the *Gérard et al.* [2002] analysis. The current density is subsequently determined by the Vlasov code. In the following sections, the value of the current density stated is that at the base of the flux tube at the ionosphere.

3.2. Solutions

[18] In order to determine the relationship between the current density and potential, the composition and temperature are held constant for all runs so that any changes in current density are a pure reflection of the variation in potential drop between the ionosphere and magnetosphere. Table 1 shows the composition and species temperatures for all runs. For an exploration on how varying the composition and temperature of the ionospheric and magnetospheric populations affects the current density, the reader is referred to *Su et al.* [2003].

[19] Figure 3 displays the densities and potential structure for a potential drop of 30 kV between the ionosphere and magnetosphere. The thin solid, dashed-dot, and dashed-dot-dot lines represent the magnetospheric electron, O^+, and S^+ densities, respectively. The bold solid and dashed lines represent the ionospheric H^+ and electron densities. The horizontal axis again represents the Jovicentric distance along the flux tube from the ionosphere to the magnetosphere. The S^+ density falls rapidly due to the centrifugal forces imposed. The O^+ population then declines with the electron population, maintaining quasi-neutrality. The potential drop occurs at $\sim$2.2 R_J which coincides with the minimum in the sum of the gravitational and centrifugal potentials (Figure 2). The ionospheric electron and ion levels are nearly identical below the potential drop, as the contribution from the high-energy tail of the magnetospheric electron population is negligible.

[20] Figure 3 (middle) displays the electric potential profile along the flux tube. A sharp potential jump occurs at $\sim$2.2 R_J. The width of the potential drop is much narrower than the resolution of the grid size, resulting in a sharp discontinuity. Below and above the large potential drop, ambipolar electric fields are set up to maintain quasi-neutrality corresponding to an ambipolar potential structure (Figure 3, bottom) of order tens to a hundred volts between the ionosphere and magnetosphere. The ambipolar potential near the equatorial plane depends on the centrifugal confinement of the ions and hence the rotation rate of the plasma. It is insensitive to the total potential drop prescribed to the system. Near the sharp potential drop, the gravitational potential overcomes the centrifugal potential (Figure 2). The ambipolar potential near the sharp drop can vary by $\sim$20 V depending on the prescribed potential difference between the ionosphere and magnetosphere. This is caused by variations in the ionospheric H^+ density at high latitudes.

[21] As the potential drop increases (from Case 1 to Case 10), the ionospheric electrons and protons become more confined to the jovian atmosphere. For example, when Φ = 100 V, the H^+ population extends $\sim$3.5 R_J along the flux tube as the tail end of the Maxwellian distribution can overcome the potential drop, traveling farther along the flux tube. The variation in the ionospheric H^+ density along the flux tube contributes to the small differences in the ambipolar potential above the sharp potential drop discussed above. The larger the potential drop prescribed, the more effective the evacuation of the auroral cavity.

[22] The potential drops and corresponding current densities are summarized in Table 2 and displayed in Figure 4. The Vlasov solution results are displayed in the insert with a dashed line and crosses. It is clear that the current density increases with increasing potential; however, the linear growth regime exists only from $\sim$300 V to $\sim$9 kV. At that point the current density plateaus, growing only slightly with increased potential drops. The solid line is the current-voltage relation corresponding to our analytic expression discussed below, and the dot-dashed line displays the current densities given by the *Knight* [1973] current-voltage relation. It is clear from Figure 4 that the *Knight* [1973] current-voltage relation does not apply. The theoretical aspects of this are discussed further in section 4.

4. Analytical Relation

[23] *Knight* [1973] derives a current-voltage relation as a steady state solution for a Maxwellian plasma with a monotonic potential between the ionosphere and plasma sheet in which the plasma density is also monotonic and only affected by mirror forces. The electron population is described as a Maxwellian and the distribution function at the magnetosphere is integrated over velocity space such that only electrons which are not trapped by magnetic mirror forces contribute to the field-aligned currents.

[24] At Jupiter, the heavy ions are confined to the equatorial plane due to large centrifugal forces. The electrons are less confined by centrifugal forces, but their mobility is impeded by an ambipolar electric field which develops to maintain quasi-neutrality along the magnetic field. The ionospheric populations are bound to the ionosphere by gravitational forces. This confinement causes a

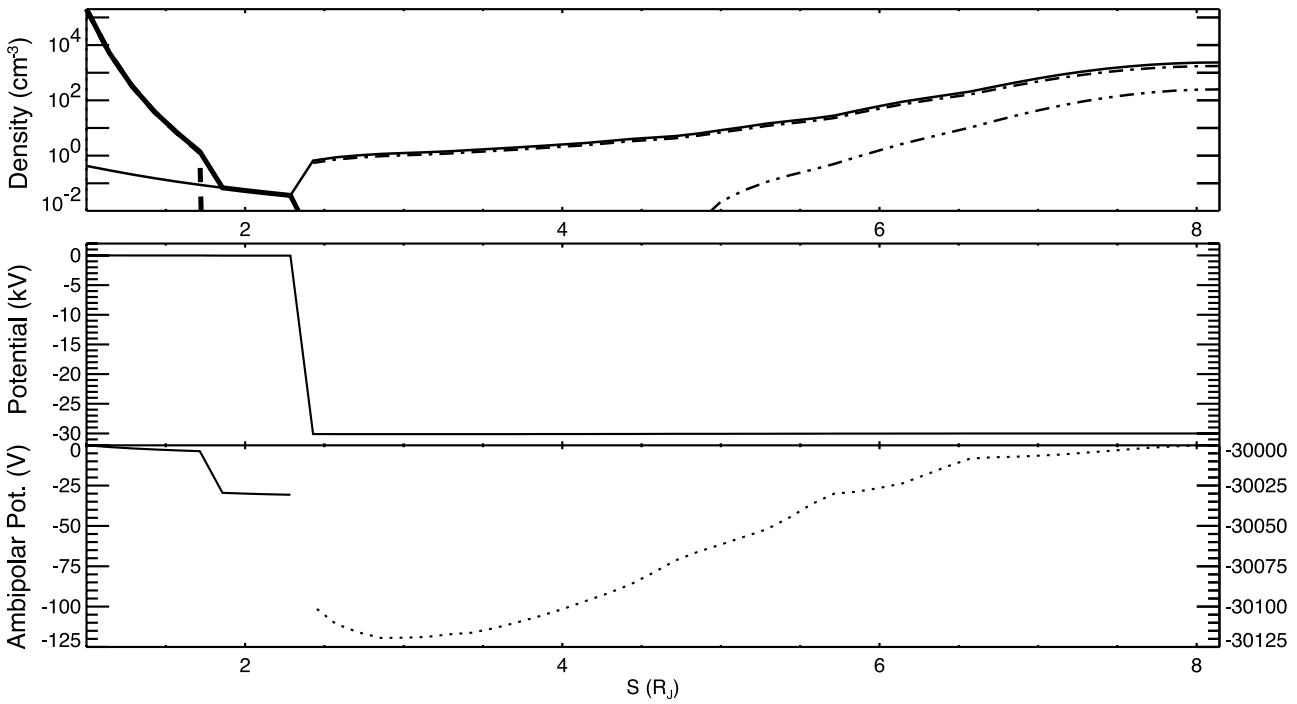

Figure 3. Densities and potential structure for Case 10. (top) The final density structure along the flux tube for the five species modeled in the Vlasov solution. An auroral cavity forms at a distance of ~2.2 R_J Jovicentric where the mirror ratio is ~8. (middle) The large-scale potential structure along the field line with a sharp drop at ~2.2 R_J. (bottom) The ambipolar structure that develops. The solid line is the ambipolar structure at the ionosphere edge of the potential drop, while the dashed line is the ambipolar structure on the magnetospheric side of the potential drop.

density depletion of current carriers at high latitudes, resulting in a 'high-latitude current choke' which limits the field-aligned currents that can flow through the system. The density distribution is nonmonotonic along the flux tube, as shown in Figure 3. In addition, the ambipolar potential increases the magnitude of the potential near the magnetosphere, resulting in a nonmonotonic potential structure between the ionosphere and plasma sheet.

[25] The critical limitation of the field-aligned current flow occurs at the point of minimum density along the flux tube and it is at this location that a significant field-aligned potential develops. In this case, the current-voltage relation resulting from the 'high-latitude current choke' is similar to that derived by *Paschmann et al.* [2003, chapter 3, equation (3.37)] as

$$j = j_x + j_x(R_x - 1)\left(1 - e^{-\left(\frac{e\Phi}{k_B T_x (R_x - 1)}\right)}\right) \qquad (3)$$

where j_x is the electron thermal current which is defined as $j_x = en_x\sqrt{\frac{T_x}{2\pi m_e}}$, R_x is the magnetic mirror ratio defined at the top of the acceleration region, T_x is the electron temperature (expressed in units of energy), n_x is the electron density at the top of the acceleration region and e is the fundamental charge. The resulting current voltage relation resembles the Earth formulation derived by *Knight* [1973]; however, there is one key difference. The 'choke' relation is based on the plasma parameters and mirror ratio at high latitudes. The electron population at high latitudes is the energetic tail of the magnetospheric population which is not as constrained by ambipolar forces. In addition, the location of the field-aligned potentials, which coincides with the position of lowest density along the flux tube, defines the magnetic mirror ratio. If the current density is below the electron thermal current, current can flow freely along the flux tube and we assume $\Phi = 0$.

[26] Figure 4 shows the 'high-latitude current choke' current-voltage relationship (solid line) and the current-voltage relationship derived by *Knight* [1973] (dot-dashed), with the results from the Vlasov solutions (dashed line with crosses) compared to the 'high-latitude current choke' current-voltage relation (solid line with stars) in the insert. The current density from the *Knight* [1973] current-voltage relation saturates when the field-aligned potential reaches ~400 kV, as opposed to ~10kV with the 'high-latitude current choke' current-voltage relation. The current-voltage relationship derived by *Knight* [1973] places the acceleration region at the equator where R_x ~400 while the 'high-latitude current choke' relationship places the acceleration region at a mirror ratio of R_x ~8. The saturated current density (~400 $\mu A/m^2$) found by the *Knight* [1973] relationship is nearly 50 times greater than that found with the 'high-latitude current choke' (~7.5 $\mu A/m^2$), grossly overestimating the field-aligned currents that flow through the Io flux tube.

[27] The 'high-latitude current choke' current-voltage relation reproduces the Vlasov solution results fairly well (Figure 4, insert), with the linear region of the current-voltage relation restricted to a potential range of ~200 V to

Table 2. Potential Drops and Current Densities for Each Case

Case	$\Phi_{\parallel}$, V	J, μA m^{-2}
1	−100	1.09
2	−200	1.42
3	−350	1.93
4	−670	3.07
5	−1,260	4.48
6	−2,400	5.67
7	−4,500	6.63
8	−8,400	7.06
9	−16,000	7.23
10	−30,000	7.28

10 kV. The current density saturates at a value equal to the mirror ratio times the electron thermal current, and is therefore limited by the location of the acceleration region. To determine the high-latitude electron properties, we modeled the magnetospheric electron distribution used in the Vlasov solutions (κ = 3), as two Maxwellians distributions. The high-latitude electron population can be described as a Maxwellian where T_{eH} = 300 eV and n_{eH} = 2 cm^{-3}, or .1% of the electron density. This is consistent with that measured by the plasma science experiment on Voyager [*Sittler and Strobel*, 1987]. R_x = 8 to represent the formation of the auroral cavity at ~2 R_J. The analytic expression and Vlasov solution are not identical as the Kappa distribution used in the Vlasov solution allows for a broader spread of energies and densities in the high-latitude electron population. However, the shape and range of current densities can be reproduced with equation (3). The Vlasov results are well approximated by the 'high-latitude current choke' current-voltage relation, which accounts for the development of the auroral cavity at high latitudes.

[28] The current-voltage relation given by equation (3) is consistent with that given by *Boström* [2003]. It is important to note that neither our analysis nor the *Boström* [2003] analysis account for the effect of trapped electrons in the auroral cavity or wave diffusion, which could further reduce the current density at the ionosphere for a given field-aligned potential.

5. Discussion and Conclusions

[29] We have presented a 'high-latitude current choke' current-voltage relation which describes the interaction of the current and field-aligned potential in a centrifugally confined plasma. We used a 1-D spatial, 2-D velocity static Vlasov code to validate this analytic formulation. The Vlasov solutions show:

[30] 1. The centrifugal forces, which result from a rapidly rotating system, confine heavy ions to the equatorial plane which in turn restrict the motion of the electrons along the flux tube as an ambipolar electric field is set up. The ambipolar potential results in a nonmonotonic potential structure between the ionosphere and magnetosphere, contrary to the assumptions of the *Knight* [1973] analysis.

[31] 2. The *Knight* [1973] current-voltage relation does not apply for a centrifugally confined plasma as it does not account for density depletions along the field line unrelated

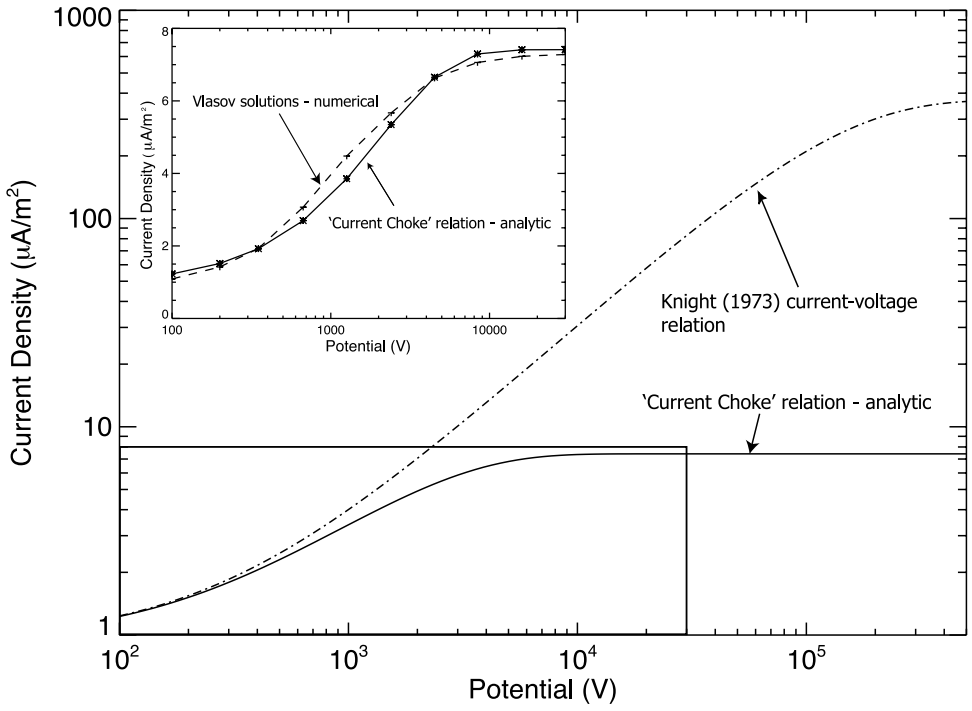

Figure 4. Current-voltage relations as derived by *Knight* [1973] (dot-dashed line) and the 'high-latitude current choke' relation (solid line). The current-voltage relationship derived by *Knight* [1973] saturates at a larger current density (~50 times larger) than the 'high-latitude current choke' relationship. The insert shows the current-voltage relation as determined by the Vlasov solution (dashed line, crosses) versus the analytic 'high-latitude current choke' current-voltage relation (solid line, stars).

to mirror forces. The density structure along the flux tube for a centrifugally confined plasma is not monotonic.

[32] 3. The resulting current-voltage relationship is nonlinear and governed by the system parameters at high latitudes where the flux tube density is at a minimum. Hence, our analytic expression depends on the high-latitude electron density, electron temperature, and the mirror ratio at the top of the acceleration.

[33] 4. The maximum field-aligned current density at the ionosphere is much less than that derived by the *Knight* [1973] analysis when the effects of the 'high-latitude current choke' are included. As a consequence, the impact of field-aligned potentials in the decoupling process for a system in which the centrifugal confinement of plasma is important need to be reexamined.

[34] 5. A sharp potential drop occurs where the sum of the gravitational and centrifugal potentials are at a minimum. This minimum is located at $\sim$2.5 R_J Jovicentric for a flux tube which intersects the equatorial plane at 5.9 R_J.

[35] **Acknowledgments.** Wolfgang Baumjohann thanks Robert Lysak and another reviewer for their assistance in evaluating this paper.

References

Bagenal, F. (1994), Empirical model of the Io plasma torus: Voyager measurements, *J. Geophys. Res.*, *99*, 11,043–11,062.

Boström, R. (2003), Kinetic and space charge control of current flow and voltage drops along magnetic flux tubes: Kinetic effects, *J. Geophys. Res.*, *108*(A4), 8004, doi:10.1029/2002JA009295.

Clarke, J. T., et al. (2002), Ultraviolet emissions from the magnetic footprints of Io, Ganymede and Europa on Jupiter, *Nature*, *415*, 997–1000.

Clarke, J. T., D. Grodent, S. W. H. Cowley, E. J. Bunce, P. Zarka, J. E. P. Connerney, and T. Satoh (2004), Jupiter's aurora, in *Jupiter: The Planet, Satellites and Magnetosphere*, pp. 639–670, Cambridge Univ. Press, Cambridge, U. K.

Crary, F. J. (1997), On the generation of an electron beam by Io, *J. Geophys. Res.*, *102*, 37–50.

Crary, F. J., F. Bagenal, L. A. Frank, and W. R. Paterson (1998), Galileo plasma spectrometer measurements of composition and temperature in the Io plasma torus, *J. Geophys. Res.*, *103*, 29,359–29,370.

Delamere, P. A., F. Bagenal, R. Ergun, and Y.-J. Su (2003), Momentum transfer between the Io plasma wake and Jupiter's ionosphere, *J. Geophys. Res.*, *108*(A6), 1241, doi:10.1029/2002JA009530.

Dols, V., J. C. Gérard, J. T. Clarke, J. Gustin, and D. Grodent (2000), Diagnostics of the Jovian aurora deduced from ultraviolet spectroscopy: Model and HST/GHRS observations, *Icarus*, *147*, 251–266.

Ergun, R. E., et al. (1998), FAST satellite observations of electric field structures in the auroral zone, *Geophys. Res. Lett.*, *25*, 2025–2028.

Ergun, R. E., C. W. Carlson, J. P. McFadden, F. S. Mozer, and R. J. Strangeway (2000), Parallel electric fields in discrete arcs, *Geophys. Res. Lett.*, *27*, 4053–4056.

Ergun, R. E., Y.-J. Su, F. Bagenal, and P. A. Delamere (2002), Recent M-I coupling discoveries and how they apply to the outer planets, paper presented at Conference on Magnetospheres of the Outer Planets, NASA, Laurel, Md.

Ergun, R. E., L. Ray, P. A. Delamere, F. Bagenal, V. Dols, and Y.-J. Su (2009), Generation of parallel electric fields in the Jupiter–Io torus wake region, *J. Geophys. Res.*, doi:10.1029/2008JA013968, in press.

Evans, D. S. (1974), Precipitating electron fluxes formed by a magnetic field aligned potential difference, *J. Geophys. Res.*, *79*, 2853–2858.

Gerard, J.-C., and V. Singh (1982), A model of energy deposition of energetic electrons and EUV emission in the Jovian and Saturnian atmospheres and implications, *J. Geophys. Res.*, *87*, 4525–4532.

Gérard, J.-C., J. Gustin, D. Grodent, P. Delamere, and J. T. Clarke (2002), Excitation of the FUV Io tail on Jupiter: Characterization of the electron precipitation, *J. Geophys. Res.*, *107*(A11), 1394, doi:10.1029/2002JA009410.

Grodent, D., and J.-C. Gérard (2001), A self-consistent model of the Jovian auroral thermal structure, *J. Geophys. Res.*, *106*, 12,933–12,952.

Knight, S. (1973), Parallel electric fields, *Planet. Space Sci.*, *21*, 741–750.

Lyons, L. R. (1980), Generation of large-scale regions of auroral currents, electric potentials, and precipitation by the divergence of the convection electric field, *J. Geophys. Res.*, *85*, 17–24.

Mauk, B. H., B. J. Anderson, and R. M. Thorne (2002), Magnetosphere-ionosphere coupling at Earth, Jupiter, and Beyond, in *Atmospheres in the Solar System: Comparative Aeronomy*, *Geophys. Monogr. Ser.*, vol. 130, AGU, Washington, D. C.

Mozer, F. S., and C. A. Kletzing (1998), Direct observation of large, quasi-static, parallel electric fields in the auroral acceleration region, *Geophys. Res. Lett.*, *25*, 1629–1632.

Paschmann, G., S. Haaland, and R. Treumann (Eds.) (2003), *Auroral Plasma Physics*, Kluwer Acad., Dordrecht, Netherlands.

Sittler, E. C., and D. F. Strobel (1987), Io plasma torus electrons: Voyager 1, *J. Geophys. Res.*, *92*, 5741–5762.

Steffl, A. J., F. Bagenal, and A. I. F. Stewart (2004), Cassini UVIS observations of the Io plasma torus. II. Radial variations, *Icarus*, *172*, 91–103.

Strobel, D. F., and S. K. Atreya (1983), Ionosphere, in *Physics of the Jovian Magnetosphere*, pp. 51–67, Cambridge Univ. Press, Cambridge, U. K.

Su, Y.-J., R. E. Ergun, F. Bagenal, and P. A. Delamere (2003), Io-related Jovian auroral arcs: Modeling parallel electric fields, *J. Geophys. Res.*, *108*(A2), 1094, doi:10.1029/2002JA009247.

Waite, J. H., T. E. Cravens, J. Kozyra, A. F. Nagy, S. K. Atreya, and R. H. Chen (1983), Electron precipitation and related aeronomy of the Jovian thermosphere and ionosphere, *J. Geophys. Res.*, *88*, 6143–6163.

F. Bagenal, P. A. Delamere, R. E. Ergun, and L. C. Ray, Laboratory for Atmospheric and Space Physics, University of Colorado, UCB392, Boulder, CO 80309-0392, USA. (lray@colorado.edu)

Y.-J. Su, Department of Physics, University of Texas at Arlington, Arlington, TX 76019, USA.